PAPER

Check for updates

AIE-active fluorescent probes as 'turn-off' sensors for the selective detection of Cr^{6+} and Fe^{3+} ions

Jiefa Shen,†[a] Jialing Mao,†[b] Xinlan Ding,†[c] Chengze Wu,[c] Shenghu Yan,*[a] Sai Zhang [ID] *[a] and Yue Zhang*[ab]

Two novel aggregation-induced emission (AIE) probes were synthesized *via* Suzuki coupling for the detection of toxic metal ions. Comprehensive characterization confirmed their structures and purity. Both compounds exhibited strong AIE behavior, providing a highly emissive platform in aqueous environments. These probes function as highly sensitive and selective 'turn-off' fluorescent sensors for Cr^{6+} and Fe^{3+} ions, respectively, *via* a distinct fluorescence quenching mechanism. Their robust response, even in the presence of competing ions, underscores their potential as reliable tools for environmental monitoring. This work highlights the utility of AIEgens as stable fluorescent platforms for designing efficient sensors for critical metal ions.

1 Introduction

The advancement of fluorescent sensors has revolutionized chemical and environmental analysis, providing powerful tools for the rapid and selective detection of hazardous metal ions.[1] Among these, chromium(VI) (Cr^{6+}) and iron(III) (Fe^{3+}) are of critical concern due to their significant environmental and biological impacts. Cr^{6+}, a pervasive pollutant from industrial processes, is a known human carcinogen and genotoxic agent, posing severe risks to human health and ecosystems.[2] Conversely, Fe^{3+} is an essential nutrient involved in oxygen transport and enzyme catalysis, but its dysregulation can lead to oxidative stress, organ damage, and its implication in various diseases.[3] Despite their importance, the simultaneous or individual detection of these specific ions using a single molecular platform remains a significant challenge and is relatively rare in the literature, primarily due to interference from other prevalent metal ions and the difficulty in designing probes with distinct binding preferences.[4]

The emergence of aggregation-induced emission (AIE) has provided a transformative strategy for designing high-performance fluorescent materials,[5] overcoming the limitations of traditional fluorophores that suffer from aggregation-caused quenching (ACQ). The pioneering work of Prof. Ben

Zhong Tang and others established that AIE-active molecules exhibit enhanced emission upon aggregation, attributed to the restriction of intramolecular motions (RIM).[6] This unique property allows for the creation of highly stable and sensitive "turn-on" or ratiometric sensors capable of operating effectively in aqueous or aggregated states, which is ideal for environmental and biological applications.[7] Recent research continues to exploit AIEgens for metal ion sensing, demonstrating their unparalleled advantages in terms of signal amplification, photostability, and applicability in complex matrices.[8]

Synthetic strategies such as Suzuki–Miyaura coupling have been widely employed to construct complex π-conjugated AIE luminogens (AIEgens) with tailored photophysical properties and binding sites.[9] These reactions enable the precise assembly of diverse biaryl and heteroaryl architectures, allowing for the systematic tuning of electronic structures and the incorporation of specific ion-recognition motifs.[10]

In this study, we address the challenge of detecting Cr^{6+} and Fe^{3+} by designing and synthesizing two novel AIE-active probes *via* Suzuki coupling. The strategic molecular design incorporates benzothiadiazole and thiophene cores, known for their electron-accepting and rigidifying properties, coupled with amide-functionalized chiral ligands to enhance selective metal ion coordination. We demonstrate that these probes exhibit pronounced AIE behavior and serve as highly sensitive and selective sensors for Cr^{6+} and Fe^{3+} ions, respectively. Their distinct and robust fluorescence responses, even in the presence of competing ions, highlight their potential as reliable tools for environmental monitoring and toxic metal detection, offering a new approach to a persistent analytical problem.

aSchool of Pharmacy, Continuous Flow Engineering Laboratory of National Petroleum and Chemical Industry, Changzhou University, Changzhou, Jiangsu Province, 213164, China. E-mail: ysh@cczu.edu.cn; zhangsai@cczu.edu.cn; zyjs@cczu.edu.cn

bSchool of Environmental Science and Engineering, Continuous Flow Engineering Laboratory of National Petroleum and Chemical Industry, Changzhou University, Changzhou, Jiangsu Province, 213164, China

cSchool of Oversea Education, Changzhou University, Changzhou, Jiangsu Province, 213164, China

† These authors have equal contribution.

2 Experimental sections

2.1. Materials and physical measurements

All chemical reagents and solvents were commercially available from Energy Chemical Co., Ltd (Shanghai, China) and of analytical grade. They were used as received without further purification unless otherwise stated. Deionized water was used for all experiments.

2.1.1 Nuclear magnetic resonance (NMR) spectroscopy. ^{1}H NMR spectra were recorded at 400 MHz on a Bruker Avance III spectrometer. Chemical shifts (δ) are reported in parts per million (ppm) relative to the residual solvent peak (CDCl$_3$: δ 7.26 ppm). Coupling constants (J) are reported in Hertz (Hz).

2.1.2 Mass spectrometry. Electrospray ionization mass spectra (ESI-MS) were acquired on a Thermo Fisher LCQ Fleet mass spectrometer.

2.1.3 UV-vis spectroscopy. Ultraviolet-visible (UV-vis) absorption spectra were measured on a Shanghai Lengguang 759S spectrophotometer using quartz cuvettes with a 1 cm path length.

2.1.4 Fluorescence spectroscopy. Steady-state fluorescence emission and excitation spectra were determined on a Shanghai Lengguang F98 fluorophotometer. A 1 cm path length quartz cuvette was used for all measurements. The slit widths for both excitation and emission were set to 5.0 nm unless specified otherwise.

2.1.5 General procedure for AIE studies. The aggregation-induced emission (AIE) properties were investigated in tetrahydrofuran (THF)/water mixtures. A stock solution of each probe (1 mM) was prepared in THF. Aliquots of this stock solution were added to cuvettes containing THF/water mixtures with varying water fractions (f_w, 0–90% v/v), maintaining a final probe concentration of 10 μM. The solutions were vortexed thoroughly and allowed to stand for 2 minutes before measurement to ensure aggregate formation.

2.1.6 General procedure for metal ion sensing. Stock solutions of metal perchlorate or chloride salts (10 mM) were prepared in deionized water. For UV-vis and fluorescence titration experiments, a stock solution of the probe (20 μM) was prepared in a PBS buffer (20 mM, pH 7.4)/THF mixture (1 : 1, v/v) to ensure the probes were in an aggregated, AIE-active state. Aliquots of the metal ion stock solutions were then added incrementally to a fixed volume of the probe solution. The solutions were mixed thoroughly and incubated for 1 minute at room temperature before each measurement. For all titration experiments, the inherent absorption of the metal ion solutions

at the excitation wavelength was eliminated by using a matched reference cell containing an identical concentration of the metal ion in the same solvent system for baseline correction. All experiments were performed at room temperature (25 ± 1 °C) (Fig. 1).

For all UV-vis and fluorescence titration experiments, the inherent absorption of the metal ion solutions was eliminated by using a matched reference cell containing an identical concentration of the metal ion in the same solvent system for baseline correction. For all fluorescence-based sensing experiments (Fig. 3–7), the probes were dissolved in a PBS buffer (20 mM, pH 7.4)/THF mixture (1 : 1, v/v).

2.2. Preparation of probe 3 and 5

The synthesis of compound **2** was carried out based on a previously published protocol.[10f] Compounds **1** and **4** were procured from commercial suppliers and utilized without further purification.

2.2.2 Synthetic procedure of proble 3. A 50 mL oven-dried round-bottom flask was filled with 4,7-dibromobenzo[c][1,2,5]thiadiazole **1** (294 mg, 1 mmol, 1 equiv.), (R)-(4-((1-phenylethyl)carbamoyl)phenyl)boronic acid (807 mg, 3 mmol, 3.0 equiv.) **2**, Pd(PPh$_3$)$_4$ (57.7 mg, 0.05 mmol), the round-bottom flask was filled with 3 mL H$_2$O and 15 mL THF. Argon was added after the round bottom flask had been vacuum-degassed. Then, for more than 48 hours, it was heated at 88 °C. Then, 150 mL H$_2$O was added, the mixture was extracted with 3 × 100 mL EA. The organic phase was combined and dried with anhydrous Na$_2$SO$_4$. The solvent was removed under reduced pressure, crude product was then purified using flash chromatography on silica gel (petroleum ether : EA, 5 : 1, v/v) to yield probe **3** as a yellow solid (274 mg, 47% yield). ESI-MS: $m/z = 583.77$ [M + H$^+$].

2.2.3 Synthetic procedure of probe 5. A 50 mL oven-dried round-bottom flask was filled with 2,5-dibromothiophene **4** (242 mg, 1 mmol, 1 equiv.), (R)-(4-((1-phenylethyl)carbamoyl)phenyl)boronic acid (807 mg, 3 mmol, 3.0 equiv.) **2**, Pd(PPh$_3$)$_4$ (57.7 mg, 0.05 mmol), K$_2$CO$_3$. The round-bottom flask was filled with 3 mL H$_2$O and 15 mL THF. Argon was added after the round bottom flask had been vacuum-degassed. Then, for more than 48 hours, it was heated at 88 °C. Then, 150 mL H$_2$O was added, the mixture was extracted with 3 × 100 mL EA. The organic phase was combined and dried with anhydrous Na$_2$SO$_4$. The solvent was removed under reduced pressure, crude product was then purified using flash chromatography on silica gel (petroleum ether : EA, 5 : 1, v/v) to yield probe **3** as a yellow solid (211 mg, 40% yield). ESI-MS: $m/z = 531.29$ [M + H$^+$].

3 Results and discussions

The aggregation-induced emission (AIE) characteristics of probes **3** and **5** were systematically investigated by monitoring their fluorescence emission spectra in THF/water mixtures with increasing water fractions (f_w) (Fig. 2). Both probes exhibited typical AIE behavior. In pure THF, a good solvent, both probes showed weak fluorescence emission due to active intramolecular rotations (IMR), a non-radiative decay pathway.
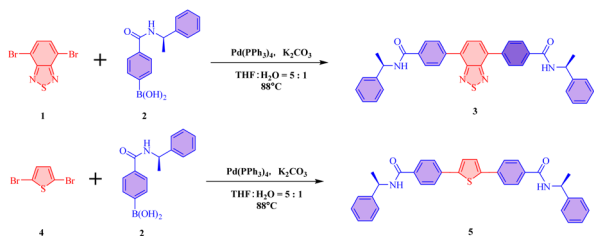

Fig. 1 Synthetic procedure of probe **3** and probe **5**.
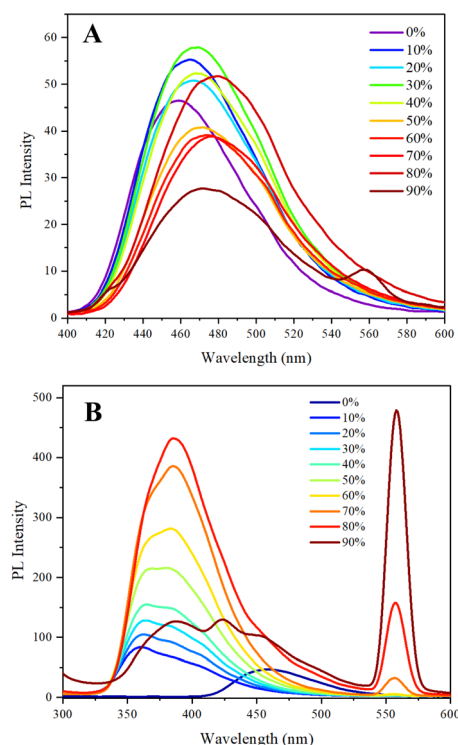
Fig. 2 (A) Fluorescence emission spectra of probe **3** in THF excited by 310 nm at different water fractions. (B) Fluorescence emission spectra of probe **5** in THF excited by 310 nm at different water fractions.

As the water fraction increased, the fluorescence behavior of both probes was consistent with the classic AIE phenomenon. In the THF-rich mixtures (f_w < 80%), the probes were likely well-dissolved, and active intramolecular rotations led to weak emission. A distinct and pronounced "turn-on" response was triggered upon reaching a critical water fraction (f_w = 80–90%), where aggregate formation occurs. For probe **3** (Fig. 2A), the fluorescence intensity at around 460 nm increased dramatically, with the maximum intensity at f_w = 90%. Similarly, probe **5** (Fig. 2B) exhibited a significant enhancement in emission intensity, culminating at f_w = 90%. This sharp enhancement at high water fractions is a hallmark of AIE and confirms that aggregation effectively restricts molecular motion, suppressing non-radiative decay and promoting radiative transition. To provide direct evidence for nanoparticle formation as the cause of the observed emission enhancement, we characterized the aggregates of probes **3** and **5** using dynamic light scattering (DLS). The DLS measurements confirmed the formation of well-dispersed nano-aggregates with average hydrodynamic diameters of 3100 nm for probe **3** and 2100 nm for probe **5** (Fig. S3 and S4) in THF/DI water mixture (50 : 50). In contrast, no significant particles were detected in pure THF solutions. This correlation between the emergence of nano-sized particles and the dramatic fluorescence enhancement provides conclusive proof of the AIE phenomenon for both probes, firmly supporting the restriction of intramolecular motion (RIM) mechanism within the aggregated state.

This emission enhancement is attributed to the restriction of intramolecular rotation (RIR) and vibration (RIV) upon aggregate formation in the water-rich, poor-solvent mixture. The aggregates restrict the molecular motion, suppressing non-radiative decay pathways and promoting radiative transition. The pronounced, discrete 'off-on' switching behavior at high water fractions confirms the successful design of both probes as AIE-active luminogens (AIEgens). This property is crucial for their application in aggregated or solid-state sensing environments, as it reduces solvent interference and improves signal stability.

The UV-visible spectra of probes **3** and **5** reveal distinct absorption characteristics, with λ_{max} values of 367 nm and 313 nm, respectively. Upon the introduction of various metal ions, noticeable variations in their respective absorption bands were observed (Fig. 3A and B). In the case of probe **3**, the absorption band exhibited a marked enhancement in intensity when exposed to Cr^{6+} ion solutions, accompanied by a pronounced tailing phenomenon (Fig. 3A). This enhancement suggests a strong interaction between the probe and Cr^{6+} ions, indicative of potential sensing capabilities. Moreover, probe **5** displayed a similar trend; its absorption band also intensified significantly upon the addition of Cr^{6+} ions, with a tailing effect that closely resembled that of probe **3**.

To improve the detection of metal ions, we conducted further investigations utilizing fluorescence emission techniques. As illustrated in Fig. 4A, probe **3** was excited at various wavelengths ranging from 280 nm to 440 nm. The data revealed that the peak emission intensity was consistently observed at
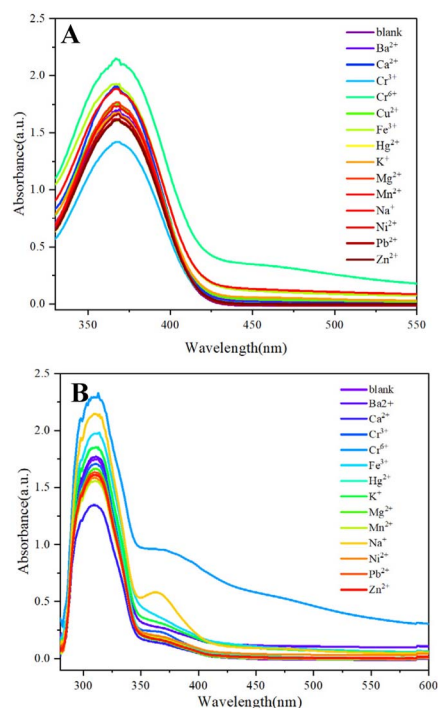

Fig. 3 (A) UV absorption spectra of **3** (1 μM) with various metal ions (0.1 μM). (B) UV absorption spectra of **5** (1 μM) with various metal ions (0.1 μM).
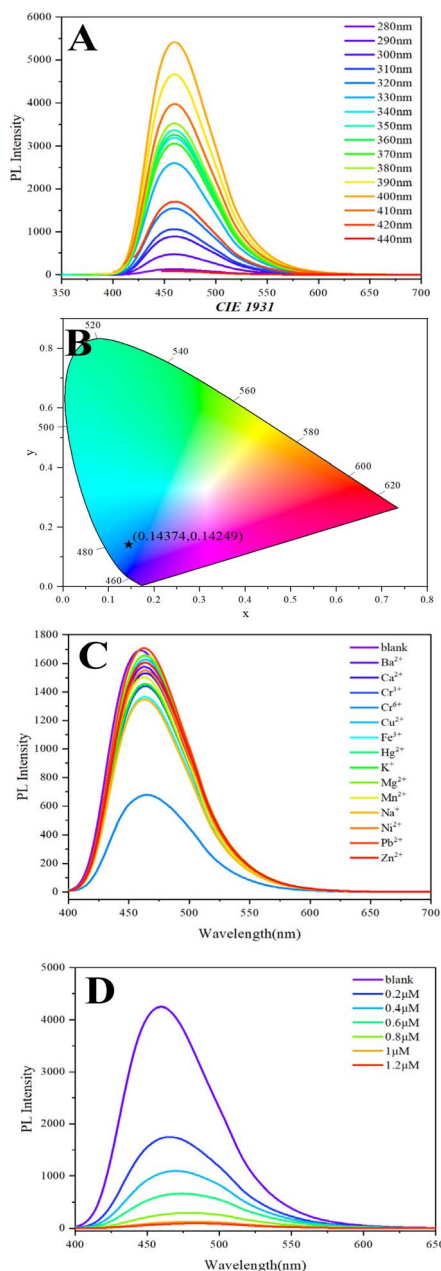
Fig. 4 (A) Fluorescence emission spectra of probe **3** excited by different excited wavelengths. (B) CIE 1931 coordinates of probe **3**. (C) Fluorescence emission spectral behavior of probe **3** (1 μM) with various metal ions (0.1 μM). (D) Concentration-dependent fluorescence emission spectra of probe **3** on the addition of various amounts of Cr^{6+} (0–1.2 μM) in PBS buffer (20 mM, pH 7.4) solution (THF). Inert: excitation wavelength is 390 nm.

probe **3**. This quenching effect was significantly more prominent than that observed with other metal ions, as demonstrated in Fig. 3C. The stark contrast in quenching behavior underscores the unique interaction between probe **3** and Cr^{6+}, suggesting that probe **3** can serve as a sensitive indicator for chromium detection. To further assess the sensitivity of the fluorescence response, we systematically measured the emission spectra of probe **3** in the presence of varying concentrations of Cr^{6+} ions. Our results indicated a stepwise quenching of emission intensity as the concentration of Cr^{6+} increased, with a notable decrease in fluorescence intensity observed as concentrations approached 1.2 μM (Fig. 4D). This concentration threshold signifies the limit at which probe **3** remains sensitive to Cr^{6+} ion interactions, revealing its potential application in detecting chromium levels in sample matrices.

In our investigation of probe **5**, we measured the emission spectra when excited by various wavelengths ranging from 280 nm to 420 nm. The behavior of probe **5** differs significantly from that of probe **3**. Notably, we observed a pronounced fluorescence red shift in probe **5**, which is evident in both the
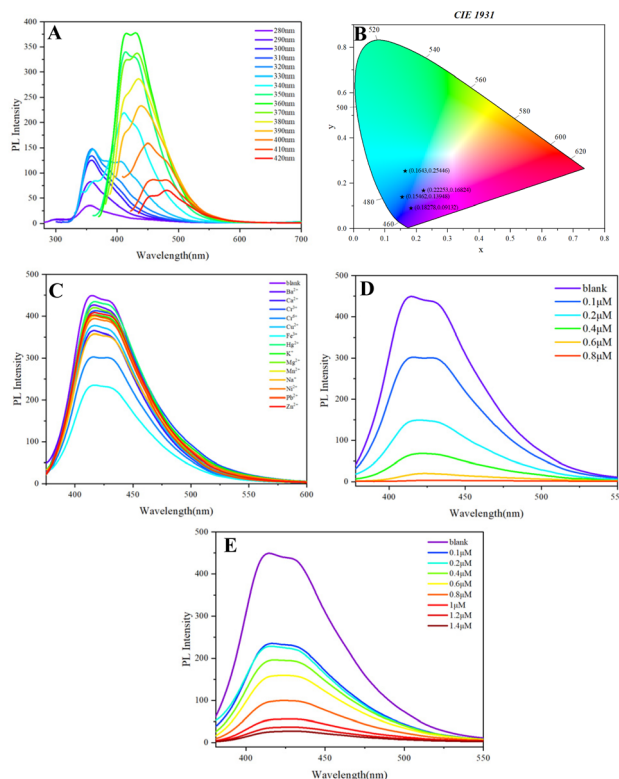

Fig. 5 (A) Fluorescence emission spectra of probe **5** excited by different excited wavelengths. Inert: 1 μM. (B) CIE 1931 coordinates of probe **5**. (C) Fluorescence emission spectral behavior of probe **5** (1 μM) with various metal ions (0.1 μM). (D) Concentration-dependent fluorescence emission spectra of probe **3** on the addition of various amounts of Cr^{6+} (0–1.2 μM) in PBS buffer (20 mM, pH 7.4) solution (THF/PBS = 1 : 9, v/v). Inert: excitation wavelength is 390 nm. (E) Concentration-dependent fluorescence emission spectra of probe **5** on the addition of various amounts of Fe^{3+} (0–1.2 μM) in PBS buffer (20 mM, pH 7.4) solution (THF/PBS = 1 : 9, v/v). Inert: excitation wavelength is 390 nm.

approximately 460 nm, irrespective of the excitation wavelength. This finding indicates a uniform emission profile across the excitation range, with corresponding luminescent chromaticities close to (0.14374, 0.14249) (Fig. 3B). Subsequently, we selected an excitation wavelength of 390 nm and proceeded to examine the effects of different metal ions at equivalent concentrations. Notably, the addition of Cr^{6+} ions resulted in a pronounced quenching phenomenon within the solution of

spectral shapes and the X-coordinates corresponding to the peak photoluminescence (PL) intensities (Fig. 5A). This shift indicates a variation in the electronic environment surrounding the probe, suggesting potential interactions that influence its fluorescent properties. Additionally, the chromatic transitions were further characterized using specific chromatic coordinates. The coordinates derived from different excitation wavelengths—(0.22253, 0.16824) for 280 nm, (0.18278, 0.09132) for 310 nm, (0.15462, 0.13948) for 400 nm, and (0.1643, 0.25446) for 410 nm—reflect the significant changes occurring in the emission profile of probe **5** (Fig. 5B). This chromatic analysis highlights the sensitivity of the probe's emission characteristics to varying excitation wavelengths.

To evaluate the effectiveness of probe **5** in metal ion detection, we introduced solutions containing various metal ions into the system. Upon adding Cr^{6+} and Fe^{3+} ions, we documented observable quenching phenomena. Specifically, the

addition of Cr^{6+} ions resulted in a reduction of approximately one-third of the PL intensity, while the presence of Fe^{3+} ions caused a more substantial quenching, exceeding 50% of the initial intensity (Fig. 5C). This differential response suggests that probe **5** has a higher affinity for Cr^{6+} ions compared to Fe(III), thus demonstrating its potential for selective sensing applications.

We also conducted concentration-dependent fluorescence emission measurements for probe **5** while systematically varying the concentrations of Cr^{6+} and Fe^{3+} ions. As illustrated in Fig. 5D, the PL intensity exhibited significant quenching at concentrations as low as 0.2 μM for Cr^{6+} ions, and further quenching was observed as the concentration approached 0.8 μM, ultimately leading to a near-complete reduction of emission intensity. This pronounced sensitivity at low concentrations underscores the feasibility of utilizing probe **5** for the detection of Cr^{6+} in environmental samples. Conversely, while Fe^{3+} ions similarly induced quenching, the response was less sensitive compared to that of Cr^{6+}. The emission intensity of probe **5** indicated noticeable quenching only upon the addition of Fe^{3+} ions at concentrations up to 1.4 μM, indicating a lower affinity or weaker interaction with this metal ion. Nevertheless, the ability of probe **5** to exhibit fluorescence quenching in response to both ions signifies its potential utility in sensing applications, albeit with differing sensitivities towards each metal.

These findings allow us to conclude that probe **5** demonstrates a significant capacity for metal ion detection, particularly for Cr^{6+} ions, characterized by dramatic changes in emission intensity upon ion addition. The unique fluorescence properties, including the observable red shift and chromatic transitions, further complement its applicability in analytical chemistry. Future investigations will delve deeper into optimizing the probe's structure for enhanced sensitivity and selectivity, as well as exploring its performance in complex matrices relevant to environmental monitoring.

This distinctive optical characteristics exhibited by probe **5**, coupled with its responsiveness to metal ion interactions, present a promising avenue for developing advanced sensing materials. The results of this study contribute to the ongoing efforts in the field of environmental detection technologies, aiming to provide effective tools for the continuous monitoring of toxic metal ions such as Cr^{6+}.

In the realm of environmental monitoring and analytical chemistry, the development of selective sensors is paramount, particularly for the detection of hazardous metal ions such as chromium (Cr^{6+}) and iron (Fe^{3+}). This study investigates the performance of two specific probes, probe **3** and probe **5**, in their ability to selectively detect these metal ions amidst a complex mixture of competing species. As illustrated in Fig. 5A and B, both probe **3** and probe **5** demonstrate promising detection capabilities for Cr^{6+} and Fe^{3+}, showcasing strong selectivity even when subjected to competitive conditions involving various metal ions. The selectivity of a sensor is critical for effective detection, as the presence of interfering ions can compromise the accuracy and reliability of the results.
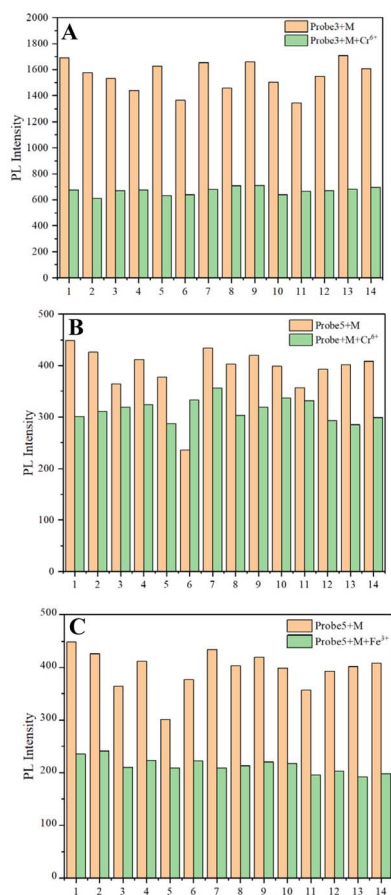

Fig. 6 (A) PL intensity changes of probe **3** (1 μM) after adding Cr^{6+} in the presence of various test cations in THF. (1) Blank; (2) Ba^{2+}, (3) Ca^{2+}; (4) Cr^{3+}; (5) Cu^{2+}; (6) Fe^{3+}; (7) Hg^{2+}; (8) K^+; (9) Mg^{2+}; (10) Mn^{2+}; (11) Na^+; (12) Ni^{2+}; (13) Pb^{2+}; (14) Zn^{2+}. (B) PL intensity changes of probe **5** (1 μM) after adding Cr^{6+} in the presence of various test cations in THF. (1) Blank; (2) Ba^{2+}, (3) Ca^{2+}; (4) Cr^{3+}; (5) Cu^{2+} (6) Fe^{3+}; (7) Hg^{2+}; (8) K^+; (9) Mg^{2+}; (10) Mn^{2+}; (11) Na^+; (12) Ni^{2+}; (13) Pb^{2+}; (14) Zn^{2+}. (C) PL intensity changes of probe **5** (1 μM) after adding Fe^{3+} in the presence of various test cations in THF. (1) Blank; (2) Ba^{2+}; (3) Ca^{2+}; (4) Cr^{3+}; (5) Cr^{6+}; (6) Cu^{2+}; (7) Hg^{2+}; (8) K^+; (9) Mg^{2+}; (10) Mn^{2+}; (11) Na^+; (12) Ni^{2+}; (13) Pb^{2+}; (14) Zn^{2+}.

For probe **3**, the selectivity remains robust when mixed with a variety of other metal ions (Fig. 3A), indicating its potential for application in real-world scenarios where multiple analytes coexist. The data suggest that probe **3** can effectively distinguish between Cr^{6+} and other metal ions, enhancing its utility in environmental assessments and analyses. In contrast, while probe **5** also demonstrates substantial selectivity for Cr^{6+} in isolation, it exhibits lower sensitivity compared to probe **3**. Notably, when probe **5** is exposed to a mixture of Cr^{6+} and Fe^{3+}, its selectivity for Cr^{6+} diminishes significantly (Fig. 5B). This loss of selectivity raises concerns regarding the reliability of probe **5** under competitive conditions, emphasizing the importance of sensitivity in achieving high-performance sensor capabilities. Furthermore, when assessing the detection of Fe^{3+}, probe **5** shows a marked improvement in selectivity relative to its performance with Cr^{6+}. Even in the presence of both Cr^{6+} and Fe^{3+}, the ability of probe **5** to preferentially detect Fe^{3+} remains evident, as indicated by the clear response observed in the measurements. This distinction highlights the differing affinities of the probes for each metal ion, revealing the complex interplay between ion specificity and sensor response.

While both probe **3** and probe **5** exhibit significant potential for detecting Cr^{6+} and Fe^{3+} ions, the performance characteristics differ considerably. Probe **3** is characterized by its strong overall selectivity and sensitivity, making it a promising candidate for detecting Cr^{6+} in mixed solutions. Conversely, probe **5**, despite its ability to detect Fe^{3+} with greater selectivity under competitive conditions, experiences a notable decrease in the sensitivity and selectivity toward Cr^{6+}. This comparison elucidates the critical attributes required for effective sensor design, particularly in applications involving environmental monitoring where the presence of multi-metallic ions is common. Future research should focus on enhancing the selectivity and sensitivity of probe **5** for Cr^{6+} detection, possibly through structural modifications or optimization of the sensing environment, to broaden its applicability and reliability in complex matrices.

To further validate the selectivity of probe **5** and rule out potential interference from counter anions, we investigated its fluorescence response to various metal ions mixed with probe **5**

Fig. 7 PL intensity changes of probe **5** (1 μM) after adding Fe^{3+} and Cr^{6+} in the presence of various test cations in THF. (1) Blank; (2) Ba^{2+}; (3) Ca^{2+}; (4) Cr^{3+}; (5) Cu^{2+}; (6) Hg^{2+}; (7) K^+; (8) Mg^{2+}; (9) Mn^{2+}; (10) Na^+; (11) Ni^{2+}; (12) Pb^{2+}; (13) Zn^{2+}.

solution containing Fe^{3+} and Cr^{6+}. As depicted in Fig. 7, the quenching efficiency of probe **5** remained consistent and pronounced upon addition of different Fe^{3+} and Cr^{6+}, even in the presence of a competitive background of common cations (Ba^{2+}, Ca^{2+}, Cr^{3+}, Cu^{2+}, Hg^{2+}, K^+, Mg^{2+}, Mn^{2+}, Na^+, Ni^{2+}, Pb^{2+}, Zn^{2+}). The negligible variation in the photoluminescence (PL) intensity changes confirms that the observed quenching is a specific result of cation recognition (Fe^{3+} or Cr^{6+}) and is independent of the associated anion. This robust performance across different combinations underscores the reliability of probe **5** for detecting the target metal ions in complex environments where various anions could be present, significantly strengthening the case for its practical application in environmental sensing.

The selective fluorescence quenching observed for probes **3** and **5** upon binding with Cr^{6+} and Fe^{3+} is rationalized by a combination of photophysical mechanisms, primarily photoinduced electron transfer (PET) and internal charge transfer (ICT). The molecular architecture of both probes is built on a donor–π–acceptor (D–π–A) framework. The benzothiadiazole core (in **3**) or the thiophene core (in **5**) serves as a strong electron-accepting (A) unit, which is conjugated to the amide-functionalized aromatic groups that act as electron-donating (D) moieties. This D–π–A design facilitates an efficient ICT transition, which is responsible for the probes' intrinsic fluorescence in their unbound state.

We propose that coordination with the highly Lewis acidic target metal ions (Cr^{6+} or Fe^{3+}) occurs primarily through the lone pairs of electrons on the carbonyl oxygen atoms of the amide groups. For probe **3**, additional weak coordination with the nitrogen atoms of the benzothiadiazole core is also plausible. This binding event significantly perturbs the electronic structure of the probe. The metal ion, acting as a potent external electron acceptor, enhances the overall electron-withdrawing strength of the acceptor unit. This is consistent with the observed red-shift and tailing in the UV-vis absorption spectra (Fig. 3), indicative of a altered ICT character.

More critically, this coordination opens a highly efficient non-radiative deactivation pathway via PET. Upon photoexcitation, an electron from the excited state of the fluorophore is transferred to the vacant, low-lying d-orbitals of the coordinated metal ion (Cr^{6+}). This process effectively quenches the fluorescence by preventing radiative recombination. The superior selectivity for Cr^{6+} and Fe^{3+} over other tested ions is attributed to their high oxidation state, strong electron affinity (high Lewis acidity), and optimal binding geometry with the pre-organized, chelating amide-based ligand environment, which thermodynamically and kinetically favors this PET process.

4 Conclusions

In conclusion, we have successfully developed two novel AIE-gens that function as highly sensitive and selective 'turn-off' fluorescent probes for the detection of Cr^{6+} and Fe^{3+} ions. The strategic molecular design, featuring rigid π-conjugated cores and amide-based recognition units, endows these probes with excellent AIE characteristics and a robust quenching response
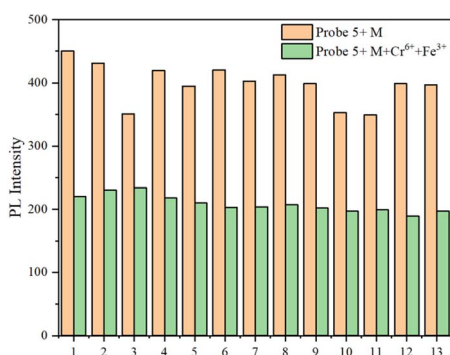
via a PET mechanism, even in competitive environments. This work underscores the significant potential of tailored AIE-active platforms for environmental monitoring of toxic metal ions. Building on this foundation, our future research will focus on leveraging multicomponent reactions[11] to efficiently construct more sophisticated AIEgens. This powerful synthetic strategy will allow for the rapid diversification of molecular structures, enabling the precise tuning of photophysical properties and binding affinities to develop next-generation fluorescent sensors with enhanced selectivity and functionality for a broader range of analytes.

Author contributions

J. S., J. M., and X. D. contributed equally to the synthesis, characterization, and sensing experiments. C. W. assisted with data analysis. S. Y., S. Z., and Y. Z. supervised the project, designed the experiments, and wrote the manuscript. All authors reviewed and approved the final manuscript.

Conflicts of interest

There are no conflicts to declare.

Data availability

Raw datasets generated during the current study are available from the corresponding authors upon reasonable request.

All data supporting the findings of this study, including experimental procedures, characterization data (NMR, mass spectrometry, UV-vis, and fluorescence spectra), and additional analytical results, are available within the article and its SI. Supplementary information is available. See DOI: https://doi.org/10.1039/d5ra05760d.

Acknowledgements

Notes and references

1 (*a*) Z. Yan, Y. Cai, J. Zhang and Y. Zhao, *Measurement*, 2022, **187**, 110355; (*b*) Y. Wang, L. He, W. Wei, X. Zhang, L. Zeng, T. Jiang, J. Li, S. Chen and Z. Gao, *Chem. Eng. J.*, 2025, **505**, 159249; (*c*) M. Qiao, L. Ding and F. Lv, *Coord. Chem. Rev.*, 2021, **432**, 213696; (*d*) S. Zhang, Q. Xu, Q. Yuan, S. Yan, Y. Zhang and G. Li, *Macromol. Rapid Commun.*, 2025, **46**, e2500090; (*e*) S. Zhang, Z. Zhang, Y. Zhang, G. Li and Z. Zhang, *Macromol. Chem. Phys.*, 2025, e00201.

2 (*a*) S. Zhang, Q. Yuan, Q. Xu, S. Yan, Y. Zhang and G. Li, *RSC Adv.*, 2025, **15**, 2242–2249; (*b*) Q. Xu, P. Chen and D. Zhang, *Hum. Reprod.*, 2025, **40**, i580; (*c*) I. C. Bordon, *Integr. Environ. Assess. Manage.*, 2023, **19**, 1411–1413.

3 (*a*) K. Jomova, S. Y. Alomar, E. Nepovimova, K. Kuca and M. Valko, *Arch. Toxicol.*, 2025, **99**, 153–209; (*b*) J. Chang, J. Mapuranga, X. Wang, H. Dong, R. Li, Y. Zhang, H. Li,

J. Shi and W. Yang, *New Phytol.*, 2024, **244**, 1947–1960; (*c*) S. Zhang, Z. Zhang, X. Qin and Z. Zhang, *Ind. Crops Prod.*, 2025, **233**, 121343; (*d*) C. Zhong, J. Yang, Y. Zhang, X. Fan, Y. Fan, N. Hua, D. Li, S. Jin, Y. Li, P. Chen, Y. Chen, X. Cai, Y. Zhang, L. Jiang, W. Yang, P. Yu and H. Lin, *Research*, 2023, **6**, 0159.

4 (*a*) T. Wu, L. Zhao, M. Ren, S. He, L. Zhang, M. Fang and B. Wang, *Environ. Sci. Technol.*, 2025, **59**, 5–10; (*b*) G. Kumar, R. Rani, K. Paul and V. Luxami, *J. Photochem. Photobiol., A*, 2019, **380**, 111845; (*c*) L. Han, X. Zhu, D. Zhang, H. Liu and B. Sun, *ACS Sens.*, 2023, **8**, 694–703; (*d*) T. Chen, S. Wei, Z. Cheng and J. Liu, *Sens. Actuators, B*, 2020, **320**, 128430; (*e*) S. Ren, M. Huang, R. Bai, L. Chen, J. Yang, J. Zhang, W. Guo, W. Ji and Y. Chen, *Research*, 2023, **6**, 0045.

5 (*a*) M. H. Chua, H. Zhou, Q. Zhu, B. Z. Tang and J. W. Xu, *Mater. Chem. Front.*, 2021, **5**, 659–708; (*b*) Z.-F. Chang, L.-M. Jing, B. Chen, M. Zhang, X. Cai, J.-J. Liu, Y.-C. Ye, X. Lou, Z. Zhao, B. Liu, J.-L. Wang and B. Z. Tang, *Chem. Sci.*, 2016, **7**, 4527–4536; (*c*) S. Saha, S. Paul, R. Debnath, N. Dey and B. Biswas, *Anal. Methods*, 2024, **16**, 1058–1068; (*d*) A. A. Bhosle, M. Banerjee and A. Chatterjee, *Sens. Diagn.*, 2024, **3**, 745–782; (*e*) R. S. Fernandes, S. Paul, J. Tydlitát, F. Bureš and N. Dey, *J. Org. Chem.*, 2024, **89**, 17926–17933.

6 (*a*) J. Mei, N. L. C. Leung, R. T. K. Kwok, J. W. Y. Lam and B. Z. Tang, *Chem. Rev.*, 2015, **115**, 11718–11940; (*b*) J. Qian and B. Z. Tang, *Chem*, 2017, **3**, 56–91; (*c*) Z. Zhou, S. Xie, X. Chen, Y. Tu, J. Xiang, J. Wang, Z. He, Z. Zeng and B. Z. Tang, *J. Am. Chem. Soc.*, 2019, **141**, 9803–9807; (*d*) H. Huang, L. Liu, J. Wang, Y. Zhou, H. Hu, X. Ye, G. Liu, Z. Xu, H. Xu, W. Yang, Y. Wang, Y. Peng, P. Yang, J. Sun, P. Yan, X. Cao and B. Z. Tang, *Chem. Sci.*, 2022, **13**, 3129–3139; (*e*) J. Luo, Z. Xie, J. W. Lam, L. Cheng, H. Chen, C. Qiu, H. S. Kwok, X. Zhan, Y. Liu, D. Zhu and B. Z. Tang, *Chem. Commun.*, 2001, 1740–1741.

7 (*a*) W. Zhu, J. Wang, K. Lei, X. Yan, J. Xu, S. Liu and C. Li, *Biosens. Bioelectron.*, 2025, **271**, 116953; (*b*) X. Kong, M. Li, Y. Zhang, Y. Yin and W. Lin, *Sens. Actuators, B*, 2021, **329**, 129232; (*c*) A. Lee, C. Song, J. J. Lee, S. S. Lee, J. Kang, K.-T. Kim and C. Kim, *J. Environ. Chem. Eng.*, 2025, **13**, 118100; (*d*) D. Banik, S. K. Manna and A. K. Mahapatra, *Spectrochim. Acta, Part A*, 2021, **246**, 119047.

8 (*a*) S. Zhang, Q. Yuan, Y. Wang, Y. Tang, A. U. Rahman, S. Jin, J. Wang, T. Xu and G. Li, *ChemistrySelect*, 2025, **10**, e01960; (*b*) L. Guo, L. Yan, R. Xie, L. Han and N. Zhu, *J. Mol. Struct.*, 2024, **1295**, 136629; (*c*) F.-Y. Ye, M. Hu and Y.-S. Zheng, *Coord. Chem. Rev.*, 2023, **493**, 215328; (*d*) Y. Li, K. Yu, H. Li, S. Li, J. Han, D.-Y. Guo, S. Chen and Q. Pan, *Anal. Chem.*, 2025, **97**, 1845–1852.

9 (*a*) S. Zhang and Z. Zhang, *Mater. Lett.*, 2025, **399**, 139051; (*b*) S. Zhang, Q. Yuan and G. Li, *RSC Adv.*, 2024, **14**, 13342–13350; (*c*) R. J. Pandhare, S. Chacko and R. M. Kamble, *J. Lumin.*, 2025, **277**, 120899; (*d*) S. Zhang, D. Chen, J.-Y. Wang, S. Yan and G. Li, *Front. Chem.*, 2023, **11**, 1259609.

10 (*a*) G. Wu, Y. Liu, Z. Yang, L. Ma, Y. Tang, X. Zhao, H. Rouh, Q. Zheng, P. Zhou, J.-Y. Wang, F. Siddique, S. Zhang, S. Jin,

Paper

RSC Advances

D. Unruh, A. J. A. Aquino, H. Lischka, K. M. Hutchins and G. Li, *Research*, 2021, **2021**, 3565791; (*b*) Y. Tang, S. Jin, S. Zhang, G.-Z. Wu, J.-Y. Wang, T. Xu, Y. Wang, D. Unruh, K. Surowiec, Y. Ma, S. Wang, C. Katz, H. Liang, Y. Li, W. Cong and G. Li, *Research*, 2022, **2022**, 9847949; (*c*) R. J. Pandhare, A. S. Gavali, P. M. Badani and R. M. Kamble, *J. Mol. Struct.*, 2025, **1342**, 142785; (*d*) Z. Su, R. Zhang, X.-Y. Yan, Q.-Y. Guo, J. Huang, W. Shan, Y. Liu, T. Liu, M. Huang and S. Z. D. Cheng, *Prog. Polym. Sci.*, 2020, **103**, 101230; (*e*) R. S. Fernandes, S. Paul and N. Dey, *Chemphyschem*, 2023, **24**, e202300434; (*f*) G. Wu, Y. Liu, Z. Yang, T. Jiang, N. Katakam, H. Rouh, L. Ma, Y. Tang, S. Ahmed, A. U. Rahman, H. Huang, D. Unruh and G. Li, *Natl. Sci. Rev.*, 2020, **7**, 588–599.

11 (*a*) X. Ma and W. Zhang, *iScience*, 2022, **25**, 105005; (*b*) X. Ma, S. Zhi and W. Zhang, *Molecules*, 2021, **26**, 1986; (*c*) X. Ma, Z. Gao, J. Niu, S. Zhang, L. Luo, S. Yan, Q. Zhang and W. Zhang, *J. Org. Chem.*, 2025, **90**, 2707–2716.